Light-Driven Self-Oscillation of Thermoplasmonic Nanocolloids

Stefano A. Mezzasalma,* Joscha Kruse, Stefan Merkens, Eneko Lopez, Andreas Seifert, Roberto Morandotti, and Marek Grzelczak*

Self-oscillation—the periodic change of a system under a non-periodic stimulus—is vital for creating low-maintenance autonomous devices in soft robotics technologies. Soft composites of macroscopic dimensions are often doped with plasmonic nanoparticles to enhance energy dissipation and generate periodic response. However, while it is still unknown whether a dispersion of photonic nanocrystals may respond to light as a soft actuator, a dynamic analysis of nanocolloids self-oscillating in a liquid is also lacking. This study presents a new self-oscillator model for illuminated colloidal systems. It predicts that the surface temperature of thermoplasmonic nanoparticles and the number density of their clusters jointly oscillate at frequencies ranging from infrasonic to acoustic values. New experiments with spontaneously clustering gold nanorods, where the photothermal effect alters the interplay of light (stimulus) with the disperse system on a macroscopic scale, strongly support the theory. These findings enlarge the current view on self-oscillation phenomena and anticipate the colloidal state of matter to be a suitable host for accommodating light-propelled machineries. In broad terms, a complex system behavior is observed, which goes from periodic solutions (Hopf–Poincaré–Andronov bifurcation) to a new dynamic attractor driven by nanoparticle interactions, linking thermoplasmonics to nonlinearity and chaos.

1. Introduction

Self-oscillation is the generation of a periodic change in a system fueled by a steady non-periodic power source.[1,2] The ability of a self-oscillator to maintain its frequency and phase enables the conversion of a steady input into a usable oscillating output, a feature that is present in many biological systems (e.g. heart beating, neuron firing).[3–6] Several synthetic materials based on liquid crystal networks,[7–11] heterostructured biomorphs[12–14] or nanoparticles-doped hydrogels[15,16] were proposed to elicit a self-sustained response under the continuous action of an external stimulus, such as light.[17,18] The ongoing increasing attention to the design and experimental development of self-oscillating matter is primarily motivated by the potential use of such systems in emerging technologies (e.g., light engines[19,20]) comprising compact components and minimum energy consumption.[21] Typically, the emergence of self-oscillations requires macroscopic dimensions (a monolith) for the host system. The reaction at the atomic/molecular level to a given stimulus needs to prompt a large-scale dissipative process, which can modulate the stimulus effect by hampering at some point the growing response (e.g., self-shadowing[15,22]). This self-limiting feedback sustains coherent oscillatory patterns on a macroscopic scale, often detectable by the naked eye. Nanoscopic lengths are too small for such a mechanism to take place, thus explaining why clustering nanoparticles were only used as colorimetric signal transducers for molecular oscillators, such as chemical

S. A. Mezzasalma
Laboratory of Optics and Optical Thin Films
Materials Physics Division
Ruđer Bošković Institute
Bijenička cesta 54, Zagreb 10000, Croatia
E-mail: smezzas@irb.hr

S. A. Mezzasalma
LINXS - Institute for advanced Neutron and X-ray Science
Lund University
Ideon Building, Delta 5 Scheelevägen 19, 223 70 Lund, Sweden

ⓘD The ORCID identification number(s) for the author(s) of this article can be found under https://doi.org/10.1002/adma.202302987

J. Kruse, M. Grzelczak
Centro de Física de Materiales (CSIC-UPV/EHU) and Donostia
International Physics Center (DIPC)
Manuel Lardizabal Ibilbidea 5, Donostia-San Sebastián 20018, Spain
E-mail: marek.g@csic.es

S. Merkens, E. Lopez, A. Seifert
CIC nanoGUNE BRTA
Tolosa Hiribidea 76, Donostia-Sebastián 20018, Spain

A. Seifert
IKERBASQUE
Basque Foundation for Science
Bilbao 48009, Spain

R. Morandotti
Institut National de la Recherche Scientifique
Centre Énergie Matériaux Télécommunications
Varennes, Québec J3X 1S2, Canada

reaction networks.[23–27] An autonomous self-oscillating colloidal system in liquid phase requires an asymmetric coupling of its periodic state with non-periodic external stimuli, a configuration lacking theoretical and experimental realizations.

The breakthrough question of this work is whether plasmonic nanoparticles—whose strong light absorption can turn them into highly efficient local heaters[28–34]—may exhibit self-oscillatory clustering by conversion of light energy into local heat. They are known to sustain self-oscillating patterns in polymer and hydrogel materials (that is, soft-actuators or soft-robots) on a macroscopic scale. Our target, instead, is creating autonomous plasmonic systems, devoid of any macromolecular matrix that are capable to self-oscillate down to the nanometer scale. To this aim, we develop a theory for energy and particle transport in an illuminated nanocolloidal dispersion, predicting the occurrence of periodic orbits via a bifurcation of the Hopf type. The experimentally realized clustering of Au nanorods (AuNRs) under uninterrupted laser irradiation highlights a self-oscillation picture at different light powers, which well agrees with our predictions. By extending the theory to embrace increasing levels of nonlinearity (such as, for instance, in the route toward chaos from Bénard problems to Lorenz-like systems[35,36]), we also detect the emergence of a new dynamic attractor.

To sum up, these findings enrich the palette of self-oscillating phenomena in soft matter by means of the rational design of stimuli-responsive photonic nanomaterials, paving the way for a nanoscale control of light-responsive processes.

2. Thermoplasmonic Nanoparticle Dynamics is Nonlinear

Our self-oscillator model relies on the following premises: i) nanoparticles undergo spontaneous aggregation in the absence of light ("dark"); ii) aggregation is reverted in dark conditions (redispersion) by homogeneous heating (**Figure 1**a); iii) the surface temperature of nanoparticles is changed by the photothermal effect; iv) the photothermal effect is enhanced by larger cluster densities (positive feedback) and is "darkened" by heat conduction/dissipation through the liquid (negative feedback) (Figure 1b). Accordingly, the cluster mass density ($Y \equiv \varrho$) and the temperature difference, between the nanoparticle surface and bulk phase ($X \equiv -\Delta T = T - T_e$), should remain mutually linked by a nonlinear dynamic system. We model nanoparticles as, at any time, they were arranged into homogeneous clusters with given state equation and number density (Section S1–S3, Supporting Information).[37] The balance laws for internal energy and particle transport in a (dilute) photoactive dispersion, illuminated at a fixed volume fraction (Φ), thus yield (Section S3.1, Supporting Information):

$$
\begin{cases}
\dot{X} = -\beta_0 \dfrac{X}{Y} + i_0 Y + a_0 \dfrac{Z}{Y}(X + T_e) - a_2 Z + p_s \dfrac{Z}{Y^2} + \eta_0 \dfrac{Z^2}{Y^3} \\
\dot{Y} = Z \\
\dot{Z} = \dfrac{Z^2}{Y} - p_0 XY - \langle \text{div } \mathbf{f} \rangle \, Y
\end{cases}
\tag{1}
$$

where $\beta_0 = k_T/(L^2 c_s)$, $i_0 = \mathcal{I}\sigma^2/(m^2 c_n)$, $a_0 = k_B/(c_s m)$, $a_2 = a/(c_s m^2)$, $p_s = P_s/c_s$, $\eta_0 = \eta_V/c_s$, $p_0 = k_B/(L^2 m)$, the dot

is the time derivative, k_T the thermal conductivity of the dispersant, m is the nanoparticle mass, $c_{s/n}$ the specific heat capacity of the dispersant/nanoparticle, a is a mean interaction term in van der Waals' state equation, σ the absorption cross-section of nanoparticles, η_v and P_s are bulk viscosity and pressure terms (relevant system quantities are in Figure 1c). A light-matter coupling is defined by $\mathcal{I} = A_n I \ell$, I being the lighting power density per surface area, ℓ the optical length and the coefficient $A_n \in (0, 1]$ evaluating the efficiency with that clusters gather nanocolloids (e.g., by an effective volume fraction $\phi = A_n \Phi$) and convert heat into work.[37,38] L denotes an energy-containing cut-off length for thermo-optical gradients (Section S2.2, Supporting Information), ranging from tens of μm upward, while $\langle \text{div } \mathbf{f} \rangle = k_B \Delta T_S/(L^2 m)$ sets $\mathbf{f}$ as a force per unit mass for interfacial heat transfer, completing the steady state definition (Section S3.2, Supporting Information):

$$
\rho_s = \frac{1}{\sigma L} \sqrt{\frac{\gamma k_T X_S}{\mathcal{I}}}, \qquad X_S = -\Delta T_S
\tag{2}
$$

here $\rho = \varrho/m$ is the number density, $\gamma = c_n/c_s$ and $\Delta T_S = T_e - T_S$ is the temperature difference between dispersant and the stationary value at the nanocolloid surface. For temperature and density oscillating in phase, Equations (2) identify the cluster where collective nanoparticle photoheating balances the heat released to the liquid (Figure 1d). Adopting $\Delta T_S \propto \sigma I/(4\pi k_T R_e)$ (R_e = equivalent spherical particle radius),[39] the thermo-optical dissipation in Equations (1) increases consistently with larger (σ/R_e^2), (k_T/c_n) and with lower mechanical inertia (i.e., m/ϕ) (Section S3.1, Supporting Information).

3. Self-Oscillation Frequencies Take Infrasonic/Acoustic Values

Another point to be addressed is if, how and at what frequency nanocolloids oscillate. Results from the linear perturbation theory in Section S3.3 (Supporting Information) predict that the stability region for the joint nanoparticle temperature and cluster density response can be expressed by only two reduced quantities, $\alpha = a/a_c$, $\xi \equiv P_s/P_{sc}$ (Figure 1e):

$$
\xi \geq \alpha + 1
\tag{3}
$$

Small perturbations to any state in Equation (3) will lead to finite (marginal stability, =) or vanishing (asymptotic stability, >) temperature and density changes. The scales $a_c = 2Q_n/(\gamma \rho_S)$, $P_{sc} = 2Q_n \rho_S/\gamma$, allowing this simple setting, rely on nanoparticle heat $Q_n = m c_n X_S$ and cluster volume $\nu_S = 1/\rho_S$, ranging typically in $a_c \approx 4 \times (10^{-9} - 10^{-2})$ J nm^3, $P_{sc} \approx 1.5 \times (10^{-1} - 10^5)$ Pa (Section S3.2, Supporting Information).

Time constants/natural frequencies stem from the roots of the secular polynomial, admitting one real negative and two imaginary eigenvalues at the marginal stability line (Equation (3)). The latter indicates a vibration with frequency ranging from infrasonic to acoustic values, $\nu_S \approx 1$ mHz to 1 kHz. In fact, expressing L through the effective volume fraction $\phi \approx m\rho_S(L)/\varrho_n$
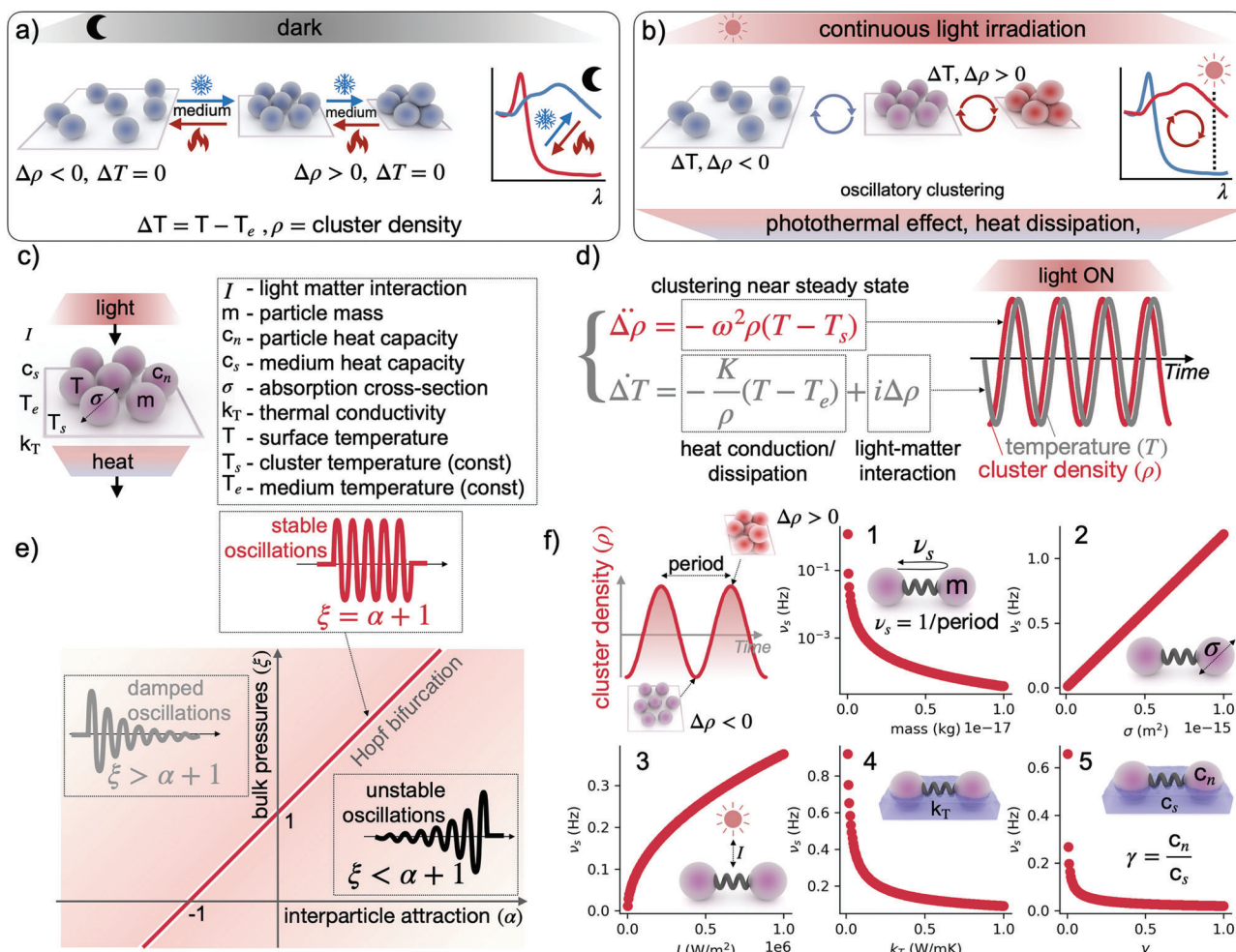
Figure 1. Phenomenology of the nanocolloid self-oscillator. a) In dark conditions, spontaneous nanoparticle aggregation/redispersion is driven by homogeneous cooling/heating. b) Under light irradiation, nanoparticle photoheating competes with heat conduction/dissipation through the environment. Thus, the number density ρ (nanoparticle number per cluster unit volume) and the temperature difference $\Delta T = T - T_e$ (between nanoparticle surface and environment) can show oscillations under uninterrupted light irradiation. c) Synopsis of relevant quantities. d) Basic oscillatory laws for clustering near the steady state (non-dimensional quantities), ω being the angular velocity, K the thermal diffusivity and i the light–matter coupling coefficient. e) Oscillation stability. In the plane of reduced interparticle attraction and bulk pressure parameters ($\alpha \times \xi$), asymptotically stable oscillation states (damped) become unstable upon crossing the line representative of stable oscillations (marginal stability) and Hopf bifurcation points (in red). f) Effect of physical parameters on the self-oscillation frequency (ν_s, Equation (4))—its value lowers with larger nanoparticle mass (m) and thermal conductivity of the dispersant (k_T), and rises with increasing light–matter interaction (absorption cross-section σ, light power density I). The larger the heat capacity ratio (nanoparticle to dispersant, $\gamma = c_n/c_s$), the smaller the frequency. As the nanoparticle thermal inertia increases relative to the inertia of the environment (a larger γ), vibrations get mechanically softer/slower (vice versa, they get stiffer/faster if the thermal inertia of the environment increases).

(ϱ_n = nanoparticle mass density) returns a first-order relationship in ϕ, i.e., (Section S3.3, Supporting Information):

$$\nu_S \approx \frac{\phi}{\pi s} \sqrt{\frac{k_B \mathcal{I}}{2\gamma m k_T}} \qquad (4)$$

Equation (4) suggests that the oscillation frequency gets larger with increasing light–matter coupling (or, implicitly, with increasing temperature difference across the solid/liquid interface), while it decreases with larger/heavier particles, the size $s = m/(\varrho_n \sigma)$ depending on the plasmon wavelength through σ. The greater the thermal inertia of nanocolloids compared to the inertia of the liquid, the smaller the frequency. A visual analysis

of Equation (4) is drawn in Figure 1f. An increase in the refractive index of the dispersant would enhance the light-nanoparticle coupling ($\mathcal{I}$) and the absorbance cross-section (σ), either increasing the self-oscillation frequency or the system stability (and vice versa, see Section S6.4).

4. Self-Oscillations and Hopf's Bifurcation

Thermoplasmonic oscillations depend on the antagonism between heat generated by light and heat released to the dispersant or, equivalently, between the work performed by clusters and the thermal inertia of solid and liquid phases. The mechanism translating this interplay into periodic solutions is non-trivial, i.e., the Hopf bifurcation, demonstrated in Section S4 (Supporting
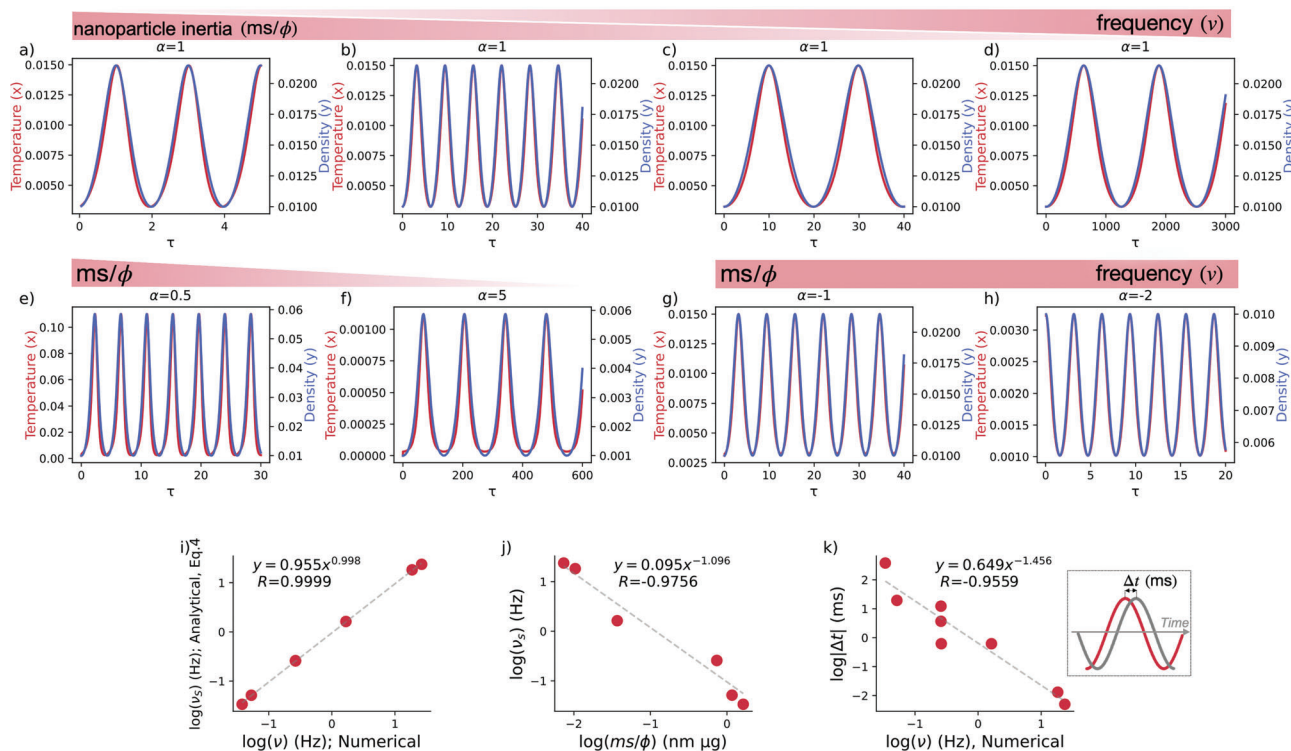
Figure 2. Marginally stable oscillations for nanoparticle temperature and cluster density. a–h) Computations of dimensionless temperature (x) and density (y) vs dimensionless time (τ) are conducted by Equations (5) near marginal stability (Figure 1e, red line). Real units can be recovered by means of t^*, T^* ϱ^*. Numerical details are in Section S5.2 (Supporting Information). By changing interparticle potential (α), one may have e.g., more spike-like profiles as in $\alpha = 1/2$ (e) or $\alpha = 5$ (f), with periodicity of ≈ 3 s (e) and ≈ 40 ms (f). g,h) Oscillations with repulsive nanoparticles are drawn in $\alpha = -1$ (g) and $\alpha = -2$ (h) at the same period (3.8 s). i) Computed frequencies ν agree with the predicted ν_s in Equation (4). j) Associated trend as a function of ms/ϕ, giving a synoptic measure of the optical/mechanical inertia. k) Absolute time lags between x and y are inversely correlated to ν. (Inset) Density peaks (y) turn out to be ahead of temperature peaks (x) (apart from (h), where they lag). Far from marginal stability, further dynamics scenarios may occur.

Information). A signature for this oscillatory regime, passive for the nanoparticle surface temperature and active for self-oscillations of the cluster density, may be deduced from the first derivative factor terms in the laws for $\ddot{\varrho}$ and $\ddot{T}$, i.e., $+(\beta_0/\varrho)\dot{T}$ and $-(\ln \dot{\varrho})\dot{\varrho}$, respectively positive and (piecewise) negative.

To inspect the oscillatory dynamics, the equation system was made dimensionless (Section S5.1, Supporting Information):

$$\begin{cases} \dot{x} = -\dfrac{x}{y} + \gamma^{-1}y - \theta_{\pm}(a)z + \chi_0\dfrac{z}{y^2} \\ \dot{y} = z \\ \dot{z} = \dfrac{z^2}{y} - \chi_1 x y + \chi_2 y \end{cases} \tag{5}$$

where $\theta_{\pm}$ is the signum function. New variables, $\tau = t/t^*$ (time), $x = X/T^*$ (temperature), $y = Y/\varrho^*$ (density), $z = Z/\beta_0$ (density time derivative), are rescaled by new units with typical orders of magnitude $t^*/|\alpha| \approx 1$ ns to 10 s, $T^*/|\alpha|^2|T \approx 10$–$10^4$ K, $\varrho^*/|\alpha| \approx 10^{-2}$ to 10^2 kg m^{-3}. Coefficients χ_k ($k = 0, 1, 2$) are interrelated through nanoparticle parameters to fulfil $\gamma \chi_2/(\chi_0 \chi_1) = |\alpha|/\xi$, and assume values $|\alpha|^3 \chi_0/\xi \approx 2.356 \times 10^{-4}$, $\chi_1/|\alpha|^4 \approx 10^{-5}$ to 10^3, $\chi_2/|\alpha|^2 \approx (10^{-7}$ to 10). Their explicit relations and influence on the thermoplasmonic response are reported in Section S5.1–S5.2 (Supporting Information).

Equations (5) are tested with reduced interparticle potential parameter in the interval $-2 \leqslant \alpha \leqslant 5$, confirming that near the locus point $\xi - \alpha = 1$ the self-oscillator model produces periodic solutions (**Figure 2**a–h). Importantly, computed frequencies agree with Equation (4), their periods changing from ≈ 40 ms to ≈ 30 s based on the extent of cluster inertia (i.e., ms/ϕ, Figure 2i–j). Numerics reveals a time lag between temperature and density varying from the µs to the 10^{-1} s scales (Figure 2k).

5. Experimental Verification of Model Predictions via Thermoplasmonic Measurements

We test our theory by devising a laser-based experimental model for oscillatory clustering of plasmonic nanoparticles (**Figure 3**a; Section S6, Supporting Information). In these conditions, the dispersion of aggregating nanoparticles gains large enough absorbance in the infrared spectral range (say, >1064 nm), where the heat production at the nanoscale induces self-redispersion (negative feedback), lowers both the photothermal effect and the local surface temperature (for more details see Section S6.3 and Figure S6, Supporting Information). The way this threshold is reached is non-trivial, depending on a competition between collective photoheating of nanoparticles and heat released to the dispersant. In this scenario nanoparticles alter their local
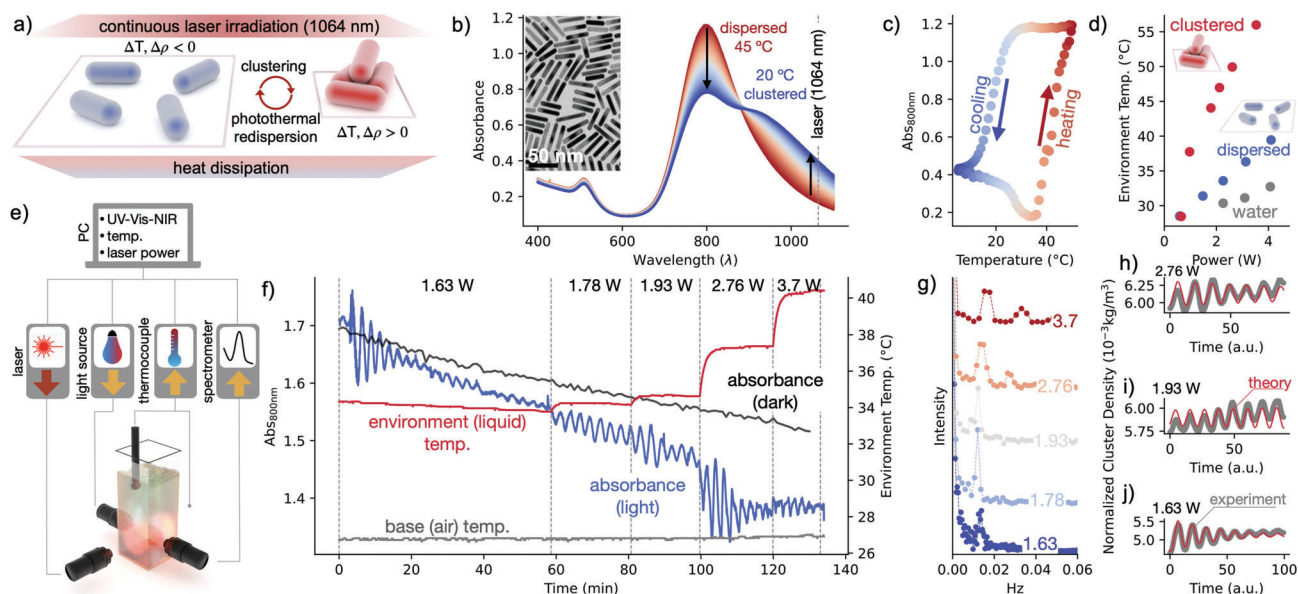
**ADVANCED
SCIENCE NEWS**

www.advancedsciencenews.com

**ADVANCED
MATERIALS**

www.advmat.de

Figure 3. Experiments. a) Scheme of experimental oscillatory clustering of plasmonic nanoparticles (AuNRs, LSPR = 800 nm) under infrared laser irradiation (wavelength = 1064 nm). b,c) Tuning the dispersion in dark conditions, where nanoparticles cluster reversibly upon lowering temperature homogeneously. b) Time-dependent UV–Vis–NIR spectra of AuNRs clustering at 20 °C in the dark (the inset shows a TEM image of AuNRs). c) Absorbance at the LSPR maximum vs base temperature in forward (cooling) and backward (heating) temperature scans, showing reversible clustering. d) Environment (dispersant) temperature vs laser power (P) for dispersed and irreversibly clustered AuNRs (bulk water used as control). e) Scheme of the experimental set-up for oscillatory clustering, featuring real-time data acquisition: environment temperature and optical response. f) Changes in the absorbance and dispersant temperature over time under continuous laser irradiation at increasing P, displaying absorbance oscillations. g) Evaluated frequency spectra for different values of P. h–j) Best fits of experimental data in the units of Equations (5) (Section S6.5, Supporting Information).

environment (surface temperature) and colloidal state (cluster density) before aggregation resumes, entailing self-oscillatory clustering.

We selected AuNRs[40] because they feature thermoplasmonic properties[41] through a localized surface plasmon resonance (LSPR) at a wavelength of ≈800 nm (Figure 3b). Our nanorods were coated with BSPP (Section S6.1.3, Supporting Information), which is known to drive spontaneous aggregation upon cooling and redispersion upon heating in accordance to a DLVO-like model for nanoparticles (Figure 3c).[37] By adjusting the salt concentration to 80 mM, the transition temperature could be set to 28 °C.[38] It is relevant to note that these two limiting states modify the optical features of the sample. Under cooling, a decrease in the plasmon band intensity (800 nm) is accompanied by an increase in the extinction coefficient at longer wavelengths (1064 nm) (Figure 3b), indicating a change in the cluster density. These trends are reversed under bulk heating (Figure 3c). Exposing dispersed or clustered AuNRs to laser illumination (1064 nm) yields a larger environment temperature (Figure 3d). Conversion of light into heat is greater in clustered states, as small interparticle distances (≈1 nm)[37] promote the formation of local hot spots by plasmon coupling. Changes in the absorbance (at the maximum of LSPR band) and bulk temperature, as compared to the dispersion in dark conditions, were monitored in real time by a thermocouple immersed in a non-irradiated region (Figure 3e). In dark states the LSPR band intensity progressively decreases (Figure 3f, black line), whereas under laser illumination the plasmon band intensity (which is strictly related to the cluster aggregation state) follows an oscillatory pattern, proving the central insight of this work (Figure 3f, blue line). Patterns vary

qualitatively with increasing laser power (P), as they are affected by the experimental conditions at a lower P. Notably, oscillation frequencies increase with larger powers, their dominant values ranging in ≈10−20 mHz when P = 1.63−3.70 W (Figure 3g). This agrees with Equation (4), giving $\nu_S \approx$ 10−50 mHz for a clustering efficiency $A_n \approx$ 0.5−1 (Section S6.1.4, Supporting Information). We also predict the temporal shape of oscillations, as it is seen from best fitting the absorbance data through the reduced mass density γ in Equations (5) (Figure 3h–j, Section S6.5, Supporting Information). As our experimental set-up has not yet straight access to thermal variations at the nanoparticle surface,[42] the measured bulk temperature remains steady for any laser power. Temperature oscillations are expected anyway, since the drastic reduction of interparticle distance increases the collective heating, especially in optically coupled nanoparticles.[28]

6. Searching for an Extended Thermoplasmonic Attractor

It is legitimate to question whether our novel self-oscillatory regime, described by Hopf periodic orbits, represents a special case of a more general dynamics.

We relaxed the strict numerical ranges in which the model parameters were evaluated, concentrating on an exploratory investigation of the equation system extended to every term hitherto omitted (see the full analysis in Section S7.1, Supporting Information). Interestingly, if such a system is written upon interparticle potential, time and (effective) mass density reversals, then one should get a phenomenological model that is characteristic of acoustic metamaterials with broad frequency response
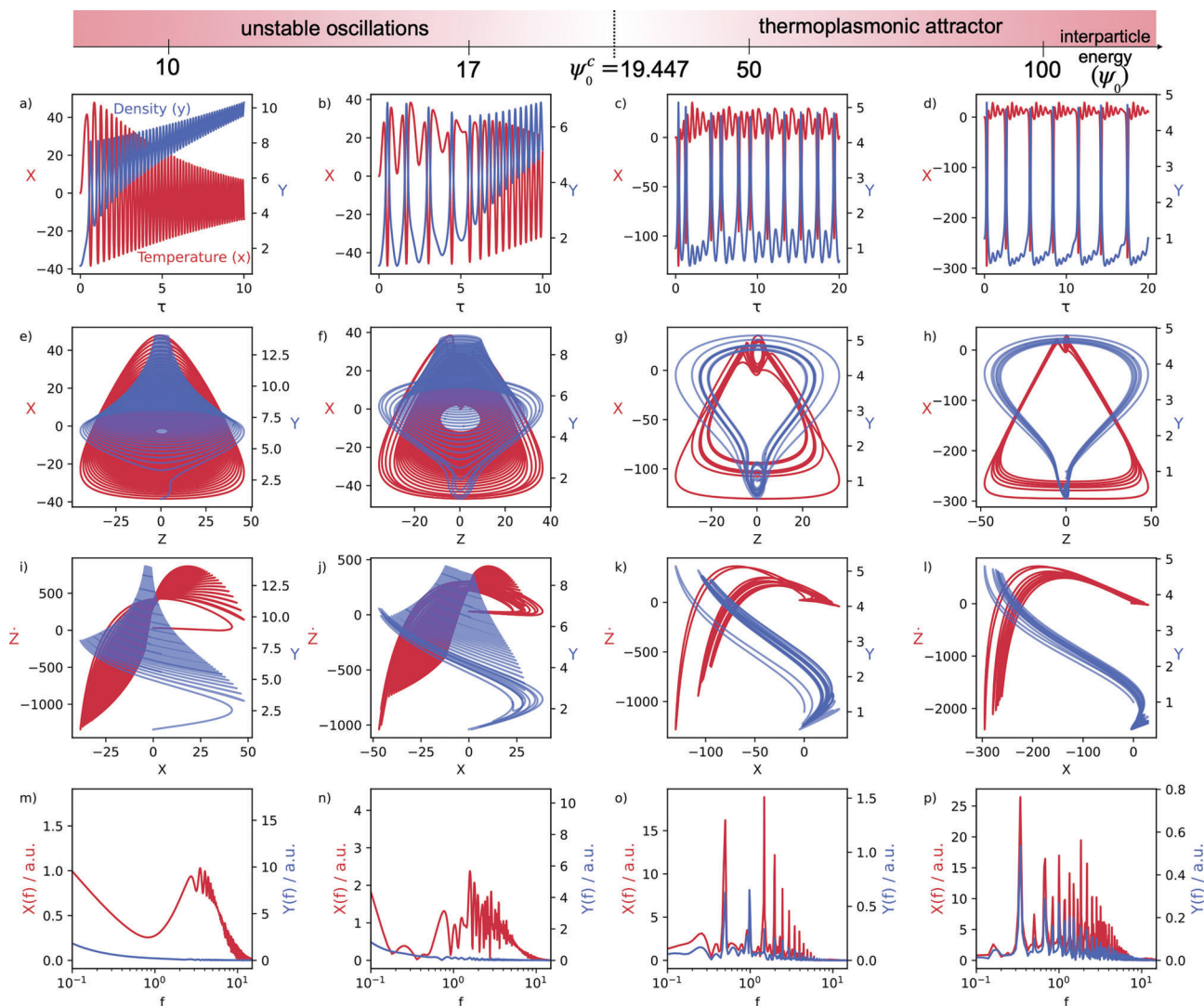
2302987 (5 of 7)

Figure 4. Emergence of a thermoplasmonic attractor. Trajectories $x = x(\tau)$, $y = y(\tau)$ (upper row), projections $x = x(z)$, $y = y(z)$ (second row) and $\dot{z} = \dot{z}(x)$, $y = y(x)$ (third row) at increasing interparticle energy parameter ψ_0. Transition from instability to a thermoplasmonic attractor occurs near $\psi_0^c \approx 19.447$. The trajectories eventually reach a subset of the state space from which, over long times, they no longer escape. Bottom row: corresponding fast Fourier transforms showing a cascade of uneven spectral lines and a sharp drop in the low-frequency tail. Quantities x, y, z, τ are the same of Figure 2 and obey the dynamic system presented in Section S7 (Supporting Information) for an extended clustering dynamics, $\dot{z} \equiv \ddot{o}$ being the second time derivative of the cluster density (Equations (7.3)). Other parameters and computational details are in Section S7.2 (Supporting Information).

(Section S7.2, Supporting Information). Trajectories were inspected for ψ_0, representative of the mean nanoparticle potential (a). As this energy descriptor increases ($\psi_0 = 1 \to 10^2$), a new attractor arises from instability (at $\psi_0^c \approx 19.447$) (**Figure 4**). Figure 4m–p illustrates how the fast Fourier transform[43] (FFT) gradually acquires a growing number of spectral lines, the low-frequency tail dropping abruptly at the transition onset (Section S7.3, Supporting Information). To obtain some more indication on the system dynamics, Lyapunov spectra[44] were computed in Section S7.4 (Supporting Information). Their maximum exponents can get positive values, suggesting a response that may be (slightly) chaotic or quasi-periodic. Further mathematical work on the self-oscillatory model and, particularly, on the new attractor hereby proposed, will improve the dynamic characterization of a thermoplasmonic system.

7. Conclusion

Self-oscillations of nanocolloids are realised by means of thermoplasmonic heating. A nonlinear model for particle and internal energy transport predicts the frequency values and temporal shape of oscillations in aqueous dispersions of gold (Au) nanorods operating as actuators under continuous light irradiation. The Hopf bifurcation explains the periodic behaviour as an antagonism between illumination and thermo-optical dissipation mediated by interparticle forces. We also predict a high-energy attractor where clusters can generate weakly chaotic or quasi-periodic patterns. The nanocolloid state of matter thus proves to be a promising means toward the design of light-propelled machinery. Controlling the nanoscale will pave the way for creating processes on a more microscopic level, suggesting

2302987 (6 of 7)

**ADVANCED
SCIENCE NEWS**

www.advancedsciencenews.com

**ADVANCED
MATERIALS**

www.advmat.de

applications beyond soft-actuators or soft-robotics, such as (bio)sensing, switchable catalysis and solar engines.

Conflict of Interest

The authors declare no conflict of interest.

Data Availability Statement

The data that support the findings of this study are available from the corresponding author upon reasonable request.

[1] A. Andronov, A. Vitt, S. Khaikin, S. Khaıkin, W. Fishwick, F. Immirzi, *Theory of Oscillators*, Dover Books on Electrical Engineering Series. Dover, Mineola, NY, USA **1987**.

[2] A. Jenkins, *Phys. Rep.* **2013**, *525*, 167.

[3] K. Kruse, F. Jülicher, *Curr. Opin. Cell Biol.* **2005**, *17*, 20.

[4] D. S. C. Damineli, M. T. Portes, J. A. Feijó, *Curr. Opin. Cell Biol.* **2022**, *77*, 102113.

[5] L. Tadrist, K. Julio, M. Saudreau, E. de Langre, *J. Fluids Struct.* **2015**, *56*, 1.

[6] T. Leclercq, N. Peake, E. de Langre, *Proc. R. Soc. A* **2018**, *474*, 20170678.

[7] A. H. Gelebart, G. Vantomme, E. W. Meijer, D. J. Broer, *Adv. Mater.* **2017**, *29*, 1606712.

[8] H. Zeng, M. Lahikainen, L. Liu, Z. Ahmed, O. Wani, M. Wang, H. Yang, A. Priimagi, *Nat. Commun.* **2019**, *10*, 5057.

[9] Z. Hu, Y. Li, J.-a. Lv, *Nat. Commun.* **2021**, *12*, 3211.

[10] M. Cheng, H. Zeng, Y. Li, J. Liu, D. Luo, A. Priimagi, Y. J. Liu, *Adv. Sci.* **2022**, *9*, 2103090.

[11] M. P. d. Cunha, M. G. Debije, A. P. H. J. Schenning, *Chem. Soc. Rev.* **2020**, *49*, 6568.

[12] X.-Q. Wang, C. F. Tan, K. H. Chan, X. Lu, L. Zhu, S.-W. Kim, G. W. Ho, *Nat. Commun.* **2018**, *9*, 3438.

[13] L. Yang, L. Chong, Y. Hu, M. Huang, Q. Ji, P. Lu, J. Liu, W. Chen, Y. Wu, *Adv. Funct. Mater.* **2020**, *30*, 15.

[14] Y. Chen, J. Yang, X. Zhang, Y. Feng, H. Zeng, L. Wang, W. Feng, *Mater. Horiz.* **2021**, *8*, 728.

[15] Y. Zhao, C. Xuan, X. Qian, Y. Alsaid, M. Hua, L. Jin, X. He, *Sci. Rob.* **2019**, *4*, eaax7112.

[16] Z. Li, N. V. Myung, Y. Yin, *Sci. Rob.* **2021**, *6*, eabi4523.

[17] Z. Chen, J. Li, Y. Zheng, *Chem. Rev.* **2022**, *122*, 3122.

[18] J. Yang, X. Zhang, X. Zhang, L. Wang, W. Feng, Q. Li, *Adv. Mater.* **2021**, *33*, 2004754.

[19] M. Li, A. Pal, A. Aghakhani, A. Pena-Francesch, M. Sitti, *Nat. Rev. Mater.* **2022**, *7*, 235.

[20] J. Li, L. Mou, Z. Liu, X. Zhou, Y. Chen, *Nat. Commun.* **2022**, *13*, 5621.

[21] B. Shen, S. H. Kang, *Matter* **2021**, *4*, 766.

[22] H. Zhang, H. Zeng, A. Eklund, H. Guo, A. Priimagi, O. Ikkala, *Nat. Nanotechnol.* **2022**, *17*, 1303.

[23] I. Lagzi, B. Kowalczyk, D. Wang, B. A. Grzybowski, *Angew. Chem., Int. Ed.* **2010**, *49*, 8616.

[24] H. Nabika, T. Oikawa, K. Iwasaki, K. Murakoshi, K. Unoura, *J. Phys. Chem. C* **2012**, *116*, 6153.

[25] R. Merindol, A. Walther, *Chem. Soc. Rev.* **2017**, *46*, 5588.

[26] B. G. van Ravensteijn, I. K. Voets, W. K. Kegel, R. Eelkema, *Langmuir* **2020**, *36*, 10639.

[27] M. Weißenfels, J. Gemen, R. Klajn, *Chem* **2021**, *7*, 23.

[28] G. Baffou, *Thermoplasmonics: Heating Metal Nanoparticles Using Light*, Cambridge University Press, Cambridge, UK **2017**.

[29] M. A. Mackey, M. R. K. Ali, L. A. Austin, R. D. Near, M. A. El-Sayed, *J. Phys. Chem. B* **2014**, *118*, 1319.

[30] S. Lal, S. E. Clare, N. J. Halas, *Acc. Chem. Res.* **2008**, *41*, 1842.

[31] F. Petronella, D. De Biase, F. Zaccagnini, V. Verrina, S.-I. Lim, K.-U. Jeong, S. Miglietta, V. Petrozza, V. Scognamiglio, N. P. Godman, D. R. Evans, M. McConney, L. De Sio, *Environ. Sci.: Nano* **2022**, *9*, 3343.

[32] A. S. Urban, T. Pfeiffer, M. Fedoruk, A. A. Lutich, J. Feldmann, *ACS Nano* **2011**, *5*, 3585.

[33] T. Kawano, Y. Niidome, T. Mori, Y. Katayama, T. Niidome, *Bioconjugate Chem.* **2009**, *20*, 209.

[34] O. Neumann, C. Feronti, A. D. Neumann, A. Dong, K. Schell, B. Lu, E. Kim, M. Quinn, S. Thompson, N. Grady, P. Nordlander, M. Oden, N. J. Halas, *Proc. Nat. Acad. Sci. USA* **2013**, *110*, 11677.

[35] E. N. Lorenz, *J. Atmos. Sci.* **1963**, *20*, 130.

[36] T. Marangoni, S. A. Mezzasalma, A. Llanes-Pallas, K. Yoosaf, N. Armaroli, D. Bonifazi, *Langmuir* **2011**, *27*, 1513.

[37] S. A. Mezzasalma, J. Kruse, A. Iturrospe, A. Arbe, M. Grzelczak, *J. Colloid Interface Sci.* **2022**, *628*, 205.

[38] J. Kruse, S. Merkens, A. Chuvilin, M. Grzelczak, *ACS Appl. Nano Mater.* **2020**, *3*, 9520.

[39] G. Baffou, P. Berto, E. Bermúdez Ureña, R. Quidant, S. Monneret, J. Polleux, H. Rigneault, *ACS Nano* **2013**, *7*, 6478.

[40] L. M. Liz-Marzán, M. Grzelczak, *Science* **2017**, *356*, 1120.

[41] L. M. Maestro, P. Haro-González, A. Sánchez-Iglesias, L. M. Liz-Marzán, J. García Solé, D. Jaque, *Langmuir* **2014**, *30*, 1650.

[42] R. Naccache, A. Mazhorova, M. Clerici, R. Piccoli, L. K. Khorashad, A. O. Govorov, L. Razzari, F. Vetrone, R. Morandotti, *Laser Photonics Rev.* **2017**, *11*, 1600342.

[43] E. Brigham, *The Fast Fourier Transform*, Prentice-Hall Signal Processing Series, Englewood Cliffs, New Jersey, **1974**, 07632.

[44] P. Manneville, in *Dissipative Structures and Weak Turbulence*, (Ed.: P. Manneville), Academic Press, Boston, MA, USA, 8**1990**, Ch. 7, pp. 247–284.